JPE 10-6-22

Dynamic Model of PEM Fuel Cell Using Real-time Simulation Techniques

Jee-Hoon Jung† and Shehab Ahmed*

†* Dept. of Electrical and Computer Eng., Texas A&M University at Qatar, Doha, Qatar

Abstract

The increased integration of fuel cells with power electronics, critical loads, and control systems has prompted recent interest in accurate electrical terminal models of the polymer electrolyte membrane (PEM) fuel cell. Advancement in computing technologies, particularly parallel computation techniques and various real-time simulation tools have allowed the prototyping of novel apparatus to be investigated in a virtual system under a wide range of realistic conditions repeatedly, safely, and economically. This paper builds upon both advancements and provides a means of optimized model construction boosting computation speeds for a fuel cell model on a real-time simulator which can be used in a power hardware-in-the-loop (PHIL) application. Significant improvement in computation time has been achieved. The effectiveness of the proposed model developed on Opal RT's RT-Lab Matlab/Simulink based real-time engineering simulator is verified using experimental results from a Ballard Nexa fuel cell system.

Key Words: PEM fuel cell, Dynamic model, Real-time simulation, Fast computation

NOMENCLATURE

α_a	Anode transfer coefficient (1.0)
α_c	Cathode transfer coefficient (0.9)
α_m	Mass transfer coefficient (0.5)
ρ_{lx}	Density of layer *x* (kg/cm^3)
σ	Stefan-Boltzmann constant (5.67 $\times$ 10^{-8} W/m^{2}K^4)
σ_c	Electrical conductivity of electrode (Ω^{-1}cm^{-1})
ε_s	Emissivity of fuel cell stack (0.9)
A_c	Cross sectional area of conductor (cm^2)
a_{120}	Electrode specific interfacial area (10^4 cm^2)
$A_{cv,f}$	Effective area of forced convection (1.27 m^2)
$A_{cv,n}$	Effective area of natural convection (7.2×10^{-3}m^2)
A_{lx}	Effective area of layer *x* (m^2)
$C_{x,y}$	Concentration of material *x* as *y* (molK)
$C_{p,lx}$	Specific heat of layer *x* (J/gK)
$C_{p,x}$	Specific heat of material *x* (J/gK)
F	Faraday's constant (96487 C)
G_f	Gibbs function in liquid form (-228170 J/mol)
h_f	Comp. coefficient for forced convection (0.01)
$h_{cv,f}$	Forced convection coefficient (W/kg)
$h_{cv,n}$	Natural convection coefficient (3.0 W/kg)
$H_{x,y}$	Enthalpy of *x* (material) as y (in/out) (J/sec)
i	Fuel cell output current density (A/cm^2)
L_c	Length of conductor (cm)
$m_{x,y}$	Anode Mass flow rate of *x* (material) as *y* (in/out) (g/sec)
M_{xg}	Mole fraction of *x* in the gas phase (H_2: 1, O_2: 0.21)
n_e	Number of electrons transferred per mol of reactant consumed (4)
P_{tg}	Total gas pressure (atm)
Q_{lxR}	Heat flow from layer *x* to the solid material
Q_{lx}	Heat flow from layer *x* to the mixed material
$Q_{res,lx}$	Heat generated by resistance in layer *x*
R	Ideal gas constant (8.314 J/molK)
R_c	Contact resistance (Ω)
T_o	Operating temperature (°C)
t_p	Effective thickness of membrane (1.83×10^{-2} cm)
T_{ca}	Temperature in the catalyst layer (K)
T_{co}	Average temperature in the flow field, gas diffusion layer, and catalyst layer (K)
T_{lx}	Borderline Temperature of layer *x* (K)
T_{amb}	Ambient temperature (K)
t_{lx}	Thickness of layer *x* (m)
U_{lx}	Overall heat transfer coefficient for layer *x*

I. INTRODUCTION

Fuel cells provide a high efficiency clean alternative to today's power generation technologies. The polymer electrolyte membrane (PEM) fuel cell has gained some acceptance in medium power commercial applications such as building backup power, grid tied distributed generation, and electric vehicles [1]. Fig. 1 is a representation of the PEM fuel cell's structure and electrochemical reactions. New control strategies

Manuscript received Apr. 20, 2010; revised Aug. 9, 2010
† Corresponding Author: jung.jeehoon@gmail.com
Tel: +974-4435-0472, Fax: +974-4423-0064, TAMUQ
* Dept. of Electrical and Computer Eng., TAMUQ, Qatar

have been developed [2], [3] for fuel cell applications [4]-[7]. The PEM fuel cell's terminal conditions demand the use of power conditioning subsystems to interface the fuel cell to its load or the grid [8], [9]. Load variations require dynamic replenishment of the air and fuel supply, while properly maintaining cell humidity and rejecting heat. Thus, the development and testing of fuel cell systems in a laboratory environment would benefit from replacing fuel cells with accurate dynamic models and hardware simulators of the complete PEM fuel cell.

One-dimensional models of thermal response and water management have been proposed for estimating the behavior of PEM fuel cell layers [10]. Dynamic fuel cell models predicting detailed internal performance using electrochemical reaction and thermal dynamic equations have been reported [11]-[14]. Model validations with commercial systems are reported [15], [16]. Computational fluid dynamic (CFD) simulations have also been used to corroborate the developed models [17].

Dynamic models based on algebraic computations have been developed for PEM fuel cell simulation [18]-[22]. The effect of ripple current was analyzed and a nonlinear controller was developed employing dynamic simulations of a fuel cell [23]. Real-time simulation of fuel cell dynamic models has been used to improve fuel cell subsystems and dc-dc converters [24], [25]. Voltage and thermal dynamic models of PEM fuel cell layers were organized and mathematical equations for computational software were proposed [26].

In this paper, real-time simulation models are proposed to emulate a PEM fuel cell in a first step towards the development of a power hardware-in-the-loop (PHIL) system similar to that shown in Fig. 2. The mathematical representation of the fuel cell electrochemistry was extracted from reference [25], [26]. Mathematical equations of the voltage loss and thermal dynamic models are programmed as simulation blocks in MATLAB Simulink. The model validation of the PEM fuel cell is achieved using experimental data extracted from a Ballard Nexa fuel cell system and recorded in publication. In order to optimize the simulation models for a real-time simulator, three methods will be proposed, which can boost computation speed of the real-time simulation. The proposed methods are minimizing algebraic calculation, separating model for parallel execution, and reducing layer structure. The proposed models are tested and verified using the RT-LAB real time engineering simulator from Opal-RT.

The main purpose of this paper is to introduce computation methods that can be employed in a multi-core processing system to increase simulation speed of a fuel cell stack. This is particularly useful in the development of a high performance PHIL system, where system bandwidth would be limited by the length of such computations. Before such a PHIL system is complete, fuel cell stack subsystem models will also be added to the model developed in this work, further contributing to the increase in simulation time. Hence, the contribution of this paper to increasing computation speed is critical to the success of upcoming work.

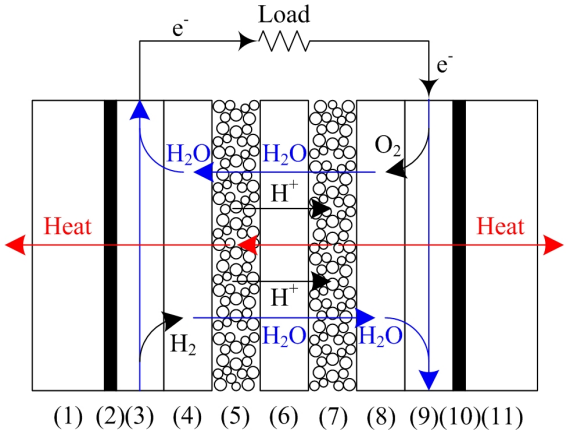

Fig. 1. Layer structure and electrochemical reactions of PEM fuel cell.

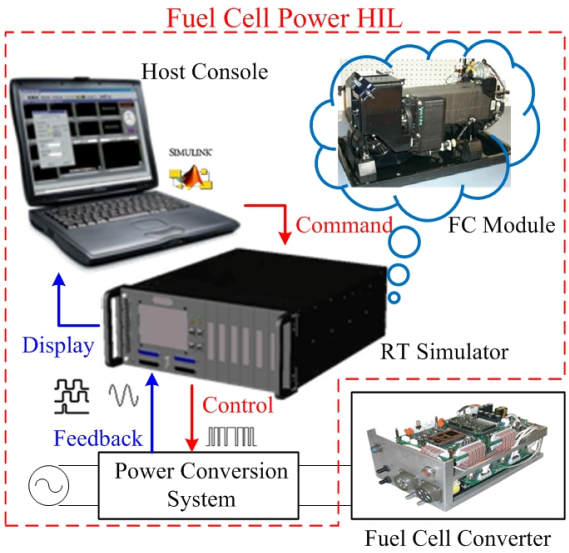

Fig. 2. Conceptual schematic of fuel cell power HIL simulation.

II. PEM Fuel Cell Terminal Voltage Model

Fig. 3 is a generalized polarization curve which shows typical voltage losses in a PEM fuel cell versus current density. The single fuel cell provides a voltage dependent on operating conditions such as temperature, electrical load, and fuel and oxidant flow rates. The maximum possible cell potential, V_c, is the net output voltage given by (1) with the reversible cell potential, V_{rv}, and the irreversible cell potential, V_{irv} [26].

$$V_c(i) = V_{rv} - V_{irv}. \tag{1}$$

The reversible cell potential, V_{rv}, can be modeled as the Nernst voltage. The irreversible voltage loss is composed of the activation overpotential V_{act}, ohmic overpotential V_{ohm}, and concentration overpotential V_{con} in (2).

$$V_{irv} = -V_{act} + V_{ohm} + V_{con}. \tag{2}$$

A. Nernst voltage model

To calculate the Nernst voltage as a reversible cell potential, the saturation pressure of water at temperature T (°C), $p_{ast}(T)$

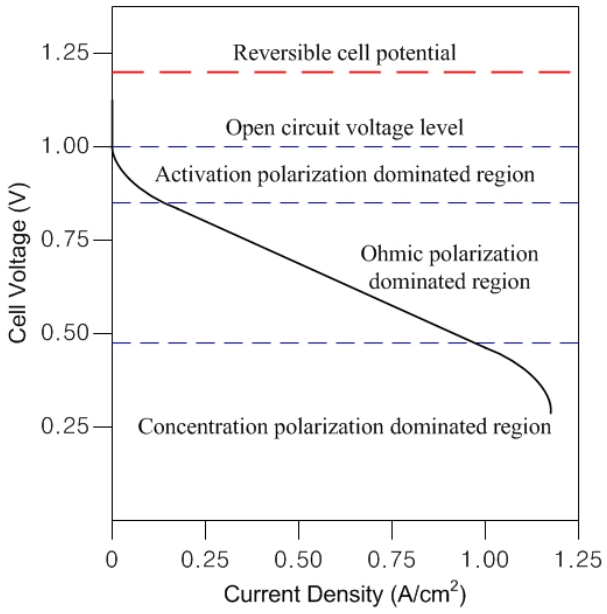

Fig. 3. Generalized polarization curve of a fuel cell.

(kgf/cm^2), and the partial pressures of hydrogen pp_{H2} and oxygen pp_{O2} are used as shown in (3) [16].

$$E_N = -\frac{G_f}{2F} - \frac{RT_o}{2F}\ln\left(\frac{p_{sat}\left(T_o\right)}{pp_{\mathrm{H2}} \times \sqrt{pp_{\mathrm{O2}}}}\right). \tag{3}$$

The saturation pressure of water can be calculated using (4).

$$\log_{10}\left[p_{sat}\left(T_o\right)\right] = -21794 + 002953T_o - 9.1837 \times 10^{-5}T_o^2 + 1.4454 \times 10^{-7}T_o^3. \tag{4}$$

B. Activation loss model

The activation loss is generated in a catalyst layer which is one of the electrode layers where electrochemical reactions occur. The activation losses at the anode and cathode of the catalyst layer can be expressed as the Tafel equation [26]:

$$V_{act} = \frac{RT_{ca}}{\alpha_c F}\left[\frac{\alpha_c}{\alpha_a + \alpha_c}\ln\left(\frac{\gamma}{i_{hr}M_{\mathrm{H2}g}}\right) - \ln\left(\frac{-\gamma}{i_{or}M_{\mathrm{O2}g}}\right)\right] \tag{5}$$

where $\gamma = i[a_{120}(1-S)P_{tg}]^{-1}$.

C. Ohmic loss model

The transport resistance of charge particles (electrons and ions) results in a voltage loss for fuel cells called ohmic loss. The electronic loss among bipolar, cooling, and contact plates is due to their contact and electrical resistance. In addition, the ionic charge losses occur in the membrane when hydrogen ions move through an electrolyte [10]. The ohmic loss can be described as follows:

$$V_{ohm} = i\left[\sum_j R_{c,j} + \sum_k \frac{L_{c,k}}{\sigma_{c,k}A_{c,k}} + \int_0^{tp}\frac{dz}{\sigma_m\left(\Delta\lambda\left(z\right)\right)}\right] \tag{6}$$

where σ_m is the conductivity profile of the membrane and $\Delta\lambda$ is the variation of the water content, respectively.

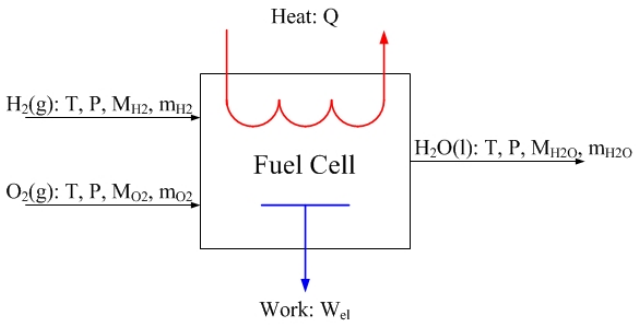

Fig. 4. Conceptual flowchart of energy balance in the fuel cell.

D. Concentration loss model

Losses due to mass transport are called concentration loss, and it can be reduced by optimizing mass transport in the flow field, gas diffusion layer, and catalyst layer [25]. To calculate total concentration loss in a PEM fuel cell, convective and diffusive mass transport in above layers should be considered. Using the Butler-Volmer equation, the concentration loss can be expressed as [26]:

$$V_{con} = \frac{RT_{co}}{n_e F}\left(1 + \frac{1}{\alpha_m}\right)\ln\left(\frac{\bar{i}_L}{\bar{i}_L - i}\right), \quad i < \bar{i}_L \tag{7}$$

where $\bar{i}_L$ is the average limiting current.

III. PEM Fuel Cell Thermal Layer Model

Performing an energy balance on the fuel cell is used to determine the proper heat distribution [10]. Energy balance on a fuel cell is based on the power production, chemical reactions, and heat loss as shown in Fig. 4. The general concept of energy balance is that the enthalpy of reactants entering the cell equals the enthalpy of products leaving the cell plus the sum of the heat generated by the power output and the rate of heat loss to the surroundings.

A. Output air temperature

The fuel cell energy balance is the sum of all the energy inputs and outputs as [26]

$$\sum_j H_{j,in} = \sum_j H_{j,out} + W_e + Q_g \tag{8}$$

where *j* is H_2, air, and H_2O/air, respectively. From the energy balance of (8), output air temperature $T_{air,out}$ of a fuel cell can be calculated as follows:

$$T_{air,out} = \frac{H_{\mathrm{H2},in} + H_{air,in} + H_{\mathrm{H2O}/air,in} - W_e - Q_g - m_{\mathrm{H2O}/air,out}h^0_{fg}}{m_{\mathrm{O2},out}C_{p,\mathrm{O2}} + m_{\mathrm{N2},out}C_{p,\mathrm{N2}} + m_{\mathrm{H2O}/air,out}C_{p,\mathrm{H2O}}} \tag{9}$$

where $H_{H2,in}$, $H_{air,in}$, $H_{H2O/air,in}$, $H_{air,out}$, and $H_{H2O/air,out}$ are enthalpies of hydrogen-in, air-in, water vapor-in air-in, air-out, vapor-out air-out, respectively.

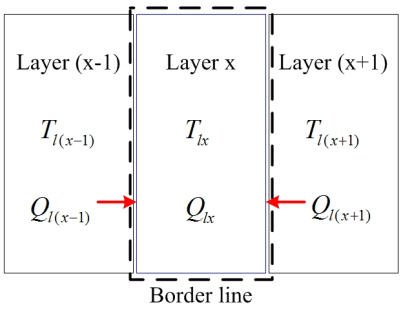

Fig. 5. General energy balance around layer x.

B. General heat transfer between two layers

Solving for heat transfer in PEM fuel cell layers is a challenge because convective, radiative, and conductive heat transfers all exist [25]. The entropic heat is generated at two layers in unequal amounts. Fig. 5 shows a general energy balance around layer x. The proposed heat transfer model ignores the variation of entropy in each layer and the thermal mass of the gas and liquid mixture to simplify its calculation. General energy balance for a fuel cell layer x can be written as [26]

$$m_{lx}\frac{dT_{lx}}{dt} = Q_{l(x-1)} + Q_{l(x+1)} \tag{10}$$

where m_{lx} is the thermal mass of the layer *x* as shown in (11).

$$m_{lx} = \rho_{lx} A_{lx} t_{lx} C_{p,lx}. \tag{11}$$

Assuming that the temperature is uniformly distributed in the layer, each heat flow can be expressed in (12).

$$\begin{aligned} Q_{l(x-1)} &= U_{l(x-1)} A_{l(x-1)} \left[T_{l(x-1)} - T_{lx}\right] \\ Q_{l(x+1)} &= U_{l(x+1)} A_{l(x+1)} \left[T_{l(x+1)} - T_{lx}\right]. \end{aligned} \tag{12}$$

C. Heat transfer in PEM fuel cell layers

The PEM fuel cell described in Fig. 1 is composed of eleven layers as follows: coolant channel (L1), gasket of anode (L2), Flow Field Plate (FFP) of anode (L3), Gas Diffusion Layer (GLD) of anode (L4), catalyst layer of anode (L5), and membrane (L6). From the seventh layer, all other cathode layers are symmetric to the anode layers till the eleventh layer. Table I shows parameters of the fuel cell layers used in the simulation. The effective area of all cell layers is 110 cm^2. These parameters are obtained from references [25], [26] and data sheets of a fuel cell power module made by Ballard Power Systems. Governing equations for heat transfer of each layer are as

1) Coolant channel:

$$m_{l1}\frac{dT_{l1}}{dt} = Q_{cv} + Q_{rad} + Q_{l2} \tag{13}$$

where Q_{cv} is the heat flow by forced and natural convection and Q_{rad} is the heat flow by radiation, respectively. They are represented as (14) and (16).

$$Q_{cv} = \left(h_{cv,n} A_{cv,n} + h_{cv,f} A_{cv,f}\right)\left(T_{amb} - T_{l1}\right) \tag{14}$$

TABLE I
MATERIAL PROPERTIES FOR CELL LAYERS

Layer	Thickness (m)	Density (kg/m^2)	Thermal conductivity (W/mK)	Heat capacity (J/kgK)
Coolant	0.001	1400	30	935
Gasket	0.001	1400	1.26	1000
FFP	0.001	1400	52	935
Diffusion	0.0004	2000	65	840
Catalyst	0.000065	387	0.2	770
Membrane	0.000183	1976	0.21	1100

$$h_{cv,f} = h_{f1}\left(h_{f2} i\right)^{hf3} \tag{15}$$

$$Q_{rad} = \sigma \varepsilon_s A_{l1}\left(T_{amb}^4 - T_{l1}^4\right). \tag{16}$$

1) Gasket:

$$m_{l2}\frac{dT_{l2}}{dt} = Q_{l1} + Q_{l3}. \tag{17}$$

2) Flow field plate:

$$m_{l3}\frac{dT_{l3}}{dt} = Q_{l2} + Q_{l2R} + Q_{l4} + Q_{l4R} + Q_{res,l3}. \tag{18}$$

3) Gas diffusion layer:

$$m_{l4}\frac{dT_{l4}}{dt} = Q_{l3} + Q_{l3R} + Q_{l5} + Q_{res,l4}. \tag{19}$$

4) Catalyst layer:

$$m_{l5}\frac{dT_{l5}}{dt} = Q_{l4} + Q_{l6} + Q_{int,l5} + Q_{res,l5}. \tag{20}$$

where $Q_{int,l5}$ is the heat generation due to the electrochemical reaction and voltage overpotential given by (21).

$$Q_{int,l5} = \left(-\frac{T_{l5}\Delta S}{n_e F} - V_{act}\right) i A_{l5} \tag{21}$$

It is noted that ΔS = 0.104 J/molK at the anode and -326.36 J/molK at the cathode. The difference in ΔS between the anode and cathode creates asymmetry in the thermal distribution within the fuel cell.

1) Membrane:

$$m_{l6}\frac{dT_{l6}}{dt} = Q_{l5} + Q_{l7} + Q_{res,l6}. \tag{22}$$

The heat generation term in the membrane consists of joule heating only.

IV. FAST COMPUTATION METHODS FOR REAL-TIME SIMULATION

The voltage loss and thermal dynamic models are implemented using Matlab/Simulink. The Simulink models are compiled using the RT-Lab real-time simulator. Fig. 6 shows the real-time simulation machine and its console monitor. The platform provides parallel computing hardware capability and accompanying transient solvers and component libraries. Optimal model construction for real-time simulation needs to take the simulator hardware architecture into consideration. In

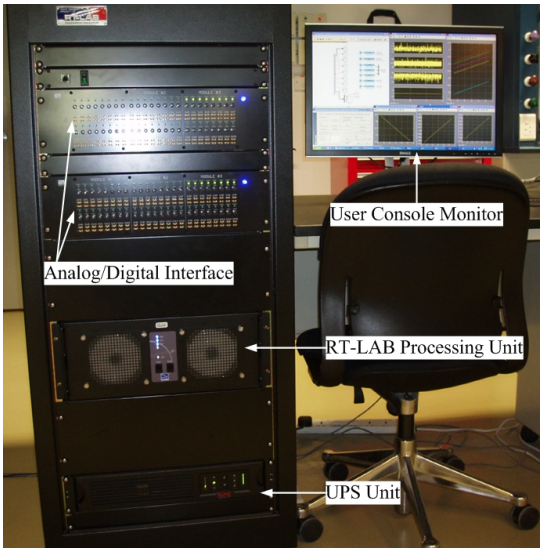

Fig. 6. Instrument photograph of RT-LAB real-time simulator.

addition, the model structures should be simplified to reduce computational burden. This section introduces the fuel cell base model development on the real-time simulator as well as the proposed approaches to reduce model computation time. These approaches are: equation construction for minimizing algebraic calculation, model distribution for a multi-core simulator, and reduced layer modeling for eliminating model redundancy.

A. Model structure for real-time simulation

The fuel cell's electrochemical equations show the strong correlation between output voltage and layer temperatures. Cell voltage is a function of pressure, current, and temperature. Pressure and current are determined by air and fuel supply as well as loading conditions. Temperature is dependent on the thermal dynamics of the fuel cell layers as well as the cooling subsystem. In addition, layer temperature is influenced by the irreversible voltage loss and cell current. The overall block diagram of the real-time simulator based fuel cell model in Fig. 7 illustrates these interdependencies.

It is composed of two major types of blocks: dynamic system blocks and monitoring/console system blocks. The dynamic system blocks consist of a thermal dynamic block and cell voltage block. Additional OpComm and OpMonitor blocks are needed by RT-LAB. The OpComm block creates a real-time communication link between the model and simulator's input/output. The OpMonitor block adds real-time monitoring capability to the simulation.

Fig. 8 shows a mathematical simulation model of the fuel cell output voltage. This model is composed of the Nernst voltage block as the reversible voltage source, the activation loss block, ohmic loss block, and concentration loss block as the irreversible voltage losses. Input cell current and output cell voltage have range limitations because the cell voltage model provides meaningful results only under proper operating voltage and current values. Fig. 9 shows a thermal dynamic simulation model of a PEM fuel cell. It is composed of a thermal dynamic system block of cell layers and an air

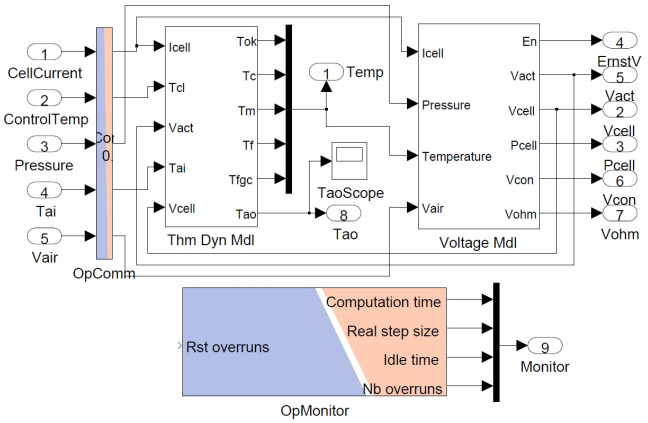

Fig. 7. PEM fuel cell dynamic model using MATLAB Simulink.

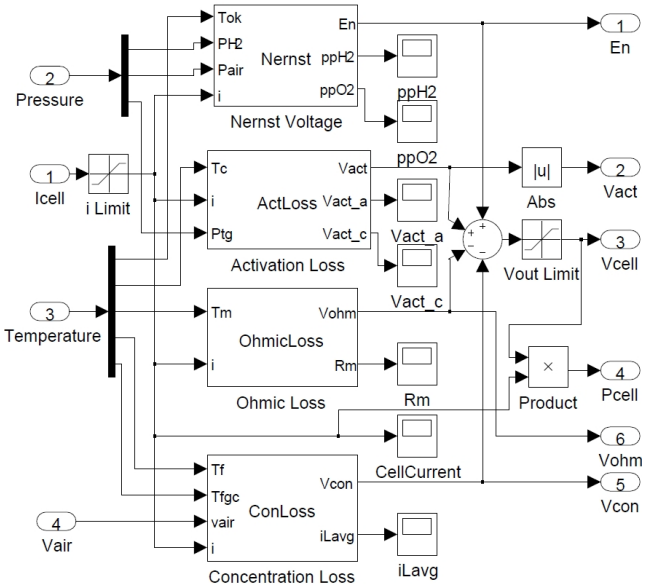

Fig. 8. Mathematical simulation model of fuel cell terminal voltage.

temperature block. Temperatures of adjacent layers become inputs of each block. Fig. 10 shows the thermal dynamic model of the catalyst layer on the anode side. From (13) to (22), thermal dynamics of layers are determined by the thermal mass, heat flow, and heat generation of each layer.

B. Model construction for minimizing algebraic calculation

The real-time simulation environment has limitations of simulator performance and computation time. The real-time simulation machine has fixed and limited processing power. The computation time is a more critical constraint because all computations should be completed within a fixed simulation time step. If not, overruns will cause errors to occur in the simulation, and they can propagate to the entire process. Minimizing algebraic calculation (MAC) is one method to enhance the simulation performance. MAC is based on extracting fixed parameters and coefficients from the model equations. Since computational results of fixed values are constant, they can be precalculated before the simulation process.

For example, the reversible voltage and all irreversible voltage losses can be simplified. Equation (7) has three variables:

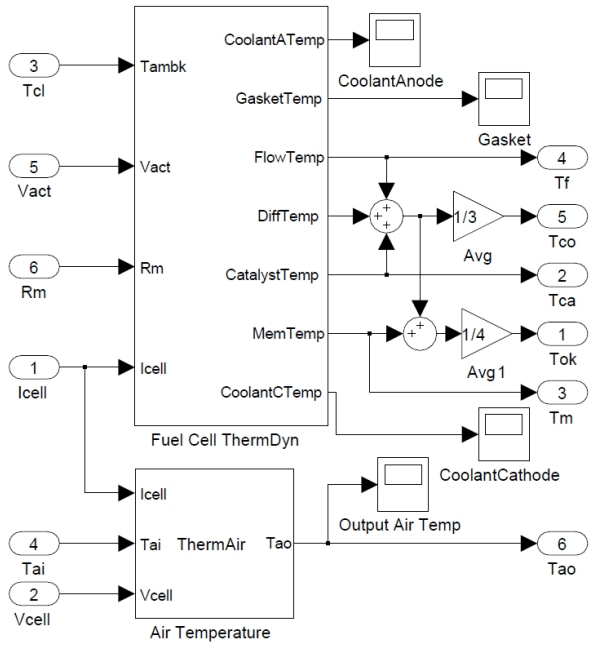

Fig. 9. Thermal dynamic simulation model of fuel cell system.

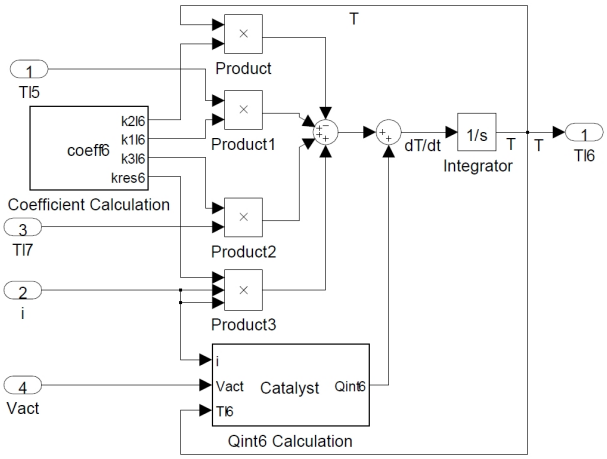

Fig. 10. Thermal dynamic model of the anode side catalyst layer.

T_{co}, i, and $\bar{i}_L$. Other coefficients are constant and determined by chemical reaction principles and physical PEM fuel cell characteristics. Therefore, (7) can be reformulated as

$$V_{con} = k_a T_{co} \ln\left(\frac{\bar{i}_L}{\bar{i}_L - 1}\right) \tag{23}$$

where $k_a = R(n_e F)^{-1}(1+\alpha_m^{-1})$. In addition, the heat transfer model of the fuel cell layers can be divided into constants and layer temperatures. From (11) and (12), equation (10) can be reformulated as shown in (24) and (25).

$$\frac{dT_{lx}}{dt} = k_{b1} T_{l(x-1)} + k_{b2} T_{l(x+1)} - (k_{b1} + k_{b2}) T_{lx} \tag{24}$$

$$\begin{aligned} k_{b1} &= m_{lx}^{-1} U_{l(x-1)} A_{l(x-1)} \\ k_{b2} &= m_{lx}^{-1} U_{l(x+1)} A_{l(x+1)}. \end{aligned} \tag{25}$$

The precalculations of the MAC method can reduce the computational burden; however, variations or modifications in the simulation model will require updates to all the pre-calculated values and the MAC structure. Therefore, model development should take this into consideration to create a user friendly model.

C. Model separation for a multi-core simulator

The RT-LAB real-time simulator setup used in this work has two Intel Core2Quad processors which have four cores each operating at 2.5 GHz. Thus, model computation speed can be improved if one makes use of the various processor cores. This is achieved by proper model separation. Simulation models should be separated so they only exchange priority signals which are state or state-derived between computation subsystems. Fig. 11 (a) shows the conventional single structure of the fuel cell dynamic model and console. There is a single master block assigned to only one core for calculating the thermal dynamics and voltage losses. Fig. 11 (b) illustrates a parallel structure separating the fuel cell terminal block and thermal dynamic block. The fuel cell terminal block is composed of the cell voltage model and stack interface model. By separating the model into master and slave subsystem blocks, the simulator can assign each model to different cores for parallel computing.

In order to maximize parallelism, the master and slave subsystems have to compute and send their outputs before they read their inputs within the same simulation step if computation nodes exchange only priority signals. The outputs are computed by migrating upstream until a dynamic state is found. If none are found, the simulation gives errors. Therefore, the state or state-derived signals have to be identified to enable parallel computation of subsystems. Fig. 12 shows the best structure for parallel execution in the real-time simulator. A state can be defined as an output computed only from preceding inputs or outputs. It means that output blocks of the master and slave subsystems, which introduce states, have to be delayed. In Fig. 10, the output state of the thermal dynamic model is naturally connected to an integrator block. So, the thermal dynamic model is suitable as a slave subsystem.

Unfortunately, in some cases simple model separation (MS) will not provide the parallel execution needed in the real-time simulation. For example, a gain block does not produce a state because its output at an arbitrary time step depends on its input at the same time step. By using the delay block, feed-through signals can be converted to priority signals. Fig. 13 shows the voltage model modified to take the proposed method into consideration. It should also be noted that delay blocks need to be handled with care since they can alter the model dynamics. Simulation results should be compared before and after to make sure that the impact of the delay block is acceptable. In the case of the proposed thermal dynamic model, the time constant of the thermal dynamics is a few minutes; thus, the impact of the delay is not significant.

The MS method is designed for multi-core simulators. Multi-core processing technology is widely used in general purpose microprocessors. Various other multi-core processing systems are currently available in the market that can make use of the model separation technique. Another commercial

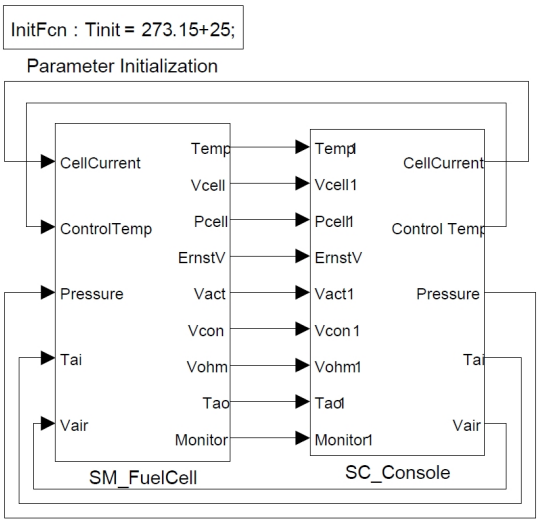

(a) Single structure

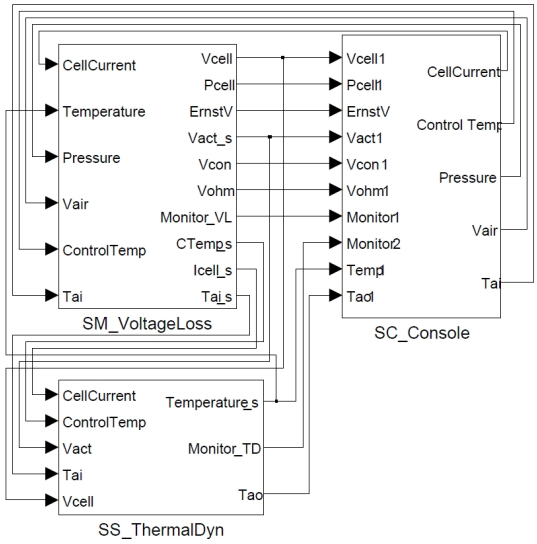

(b) Parallel computation structure

Fig. 11. Separation of the simulation model.

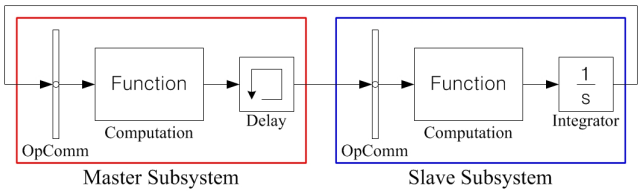

Fig. 12. Parallel computation structure of the simulation model.

real-time simulator, RTDS, supports parallel processing using multi-core processors. Additionally, dSpace, which is a generic real-time simulator, also supports parallel processing.

D. Reduced layer model of PEM fuel cell

In Fig. 1, one can see that the anode and cathode layer structures of the PEM fuel cell are almost symmetric around a membrane. From (21), the difference between the anode and cathode layers is only the heat generation by the electrochemical reaction in the catalyst layer. The base model needs to compute all eleven thermal dynamic blocks within a single

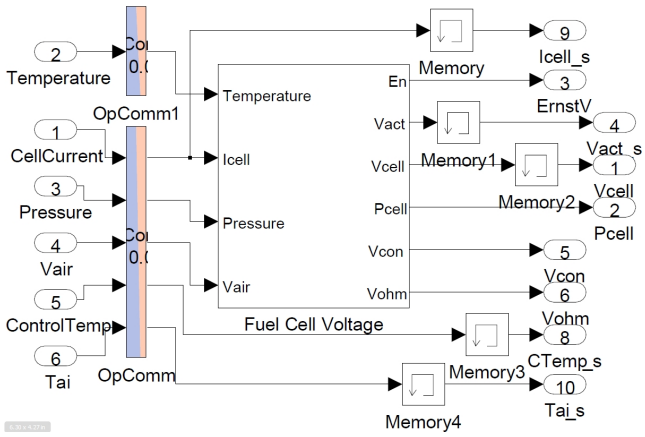

Fig. 13. Fuel cell voltage model for parallel computation.

time step. If the model of cell layers is simplified using the fuel cell symmetry, computational burden can be reduced. Fig. 14 shows a reduced layer (RL) structure of the simulation model. In Fig. 14, only seven blocks instead of eleven are required to compute the fuel cell dynamics.

This RL model is generated using an approximation of the catalyst asymmetry between the anode and cathode. In Fig. 14, the feedback temperature of the gas diffusion layer is taken as the average temperature of the anode and cathode catalyst layers. This approximation induces slight errors in the calculation results of layer temperatures.

V. Results

In this section, performance of the voltage loss and thermal dynamic models are discussed. The fuel cell output voltage and power are illustrated according to the current density and operating temperature. Thermal dynamics and steady state temperatures of the layers are also presented. The proposed fast computation methods MAC, MS, and RL, are verified by simulation results using the RT-LAB real-time simulator.

A. Model characteristics

Fig. 15 shows cell output voltage and power graphs of the fuel cell voltage model. According to the fuel cell's voltage loss model, the output voltage changes for varying operating temperature and current density. In the low temperature region, the voltage linearly decreases for increasing current density. However, the voltage decreases steeply with increasing current density in the high temperature region. In addition, the voltage increases proportionally to temperature in the low current region, and drastically collapses when the temperature increases in the high current region. Therefore, the cell output power has a maximum value around the point of 0.5 A/cm^2 and 90°C.

Fig. 16 shows temperature graphs of the fuel cell layers. Fig. 16 (a) shows transient thermal performance of a cell evolving over 20 minutes. Initial cell temperature was set to 25 °C and load current was assigned to 40 A. Fig. 16 (b) shows temperatures in all layers 20 minutes into the simulation. Characters A and C represent the anode and cathode, respectively. The cathode catalyst has the highest temperature because of high a ΔS in (21). The temperature

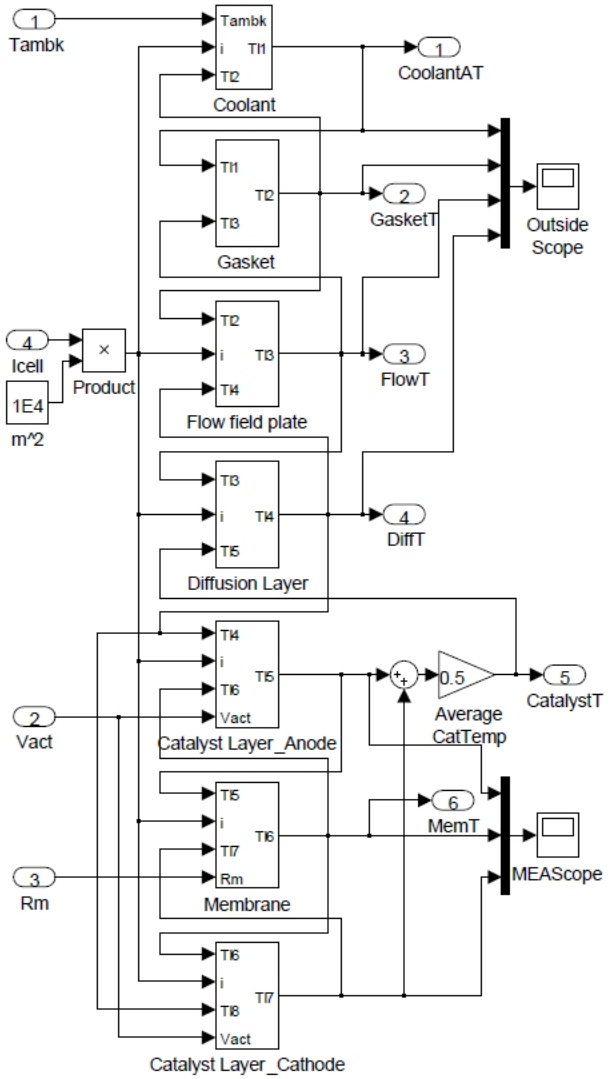

Fig. 14. Reduced layer structure of simulation model.

difference between the conventional and reduced layer model did not exceed 0.26 °C.

B. Model validation test

Validation of the proposed fuel cell output voltage model was done using experimental data recorded in reference [16]. The data was obtained on a BPS Nexa power module for two operating temperatures 45 °Cand 65 °C. Fig. 17 shows the similarity between the experimental data and the polarization curve of the voltage model at both temperatures. At 65 °C, two cell voltage data points at current densities of 0.3 and 0.4 A/cm^2 have larger differences between simulated and experimental results when compared to the rest of the data. It is expected that these differences come from the operation of the fuel cell system used in the experiment. Subsystems such as fuel and air supply, compressor, and cooler operate under the control of the system controller; this control depends on the conditions of the stack system, whereas, our current model only addresses the fuel cell. Further work by the team is geared towards the complete system development, which should enable detailed analysis of such differences. However,

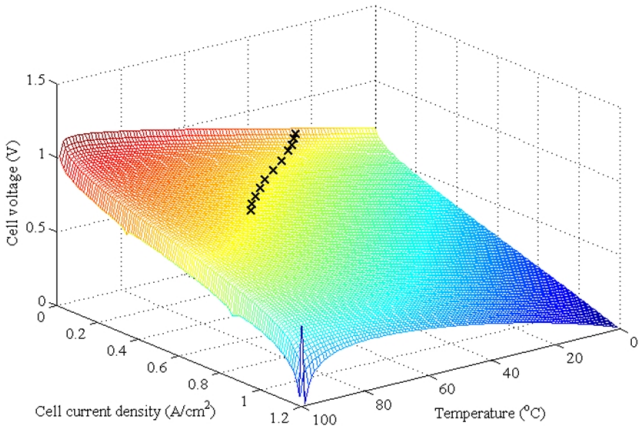

(a) Cell voltage.

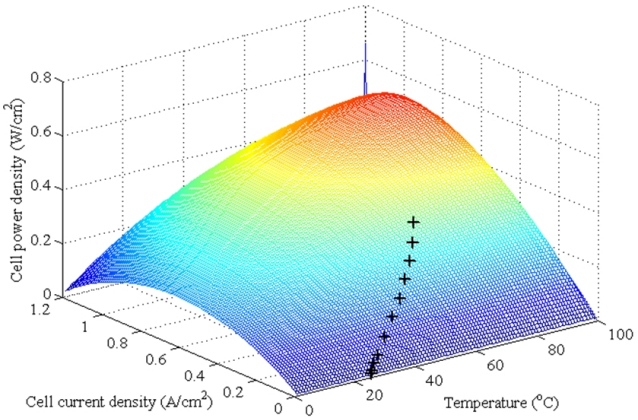

(b) Cell power density.

Fig. 15. Output characteristics of the fuel cell voltage model.

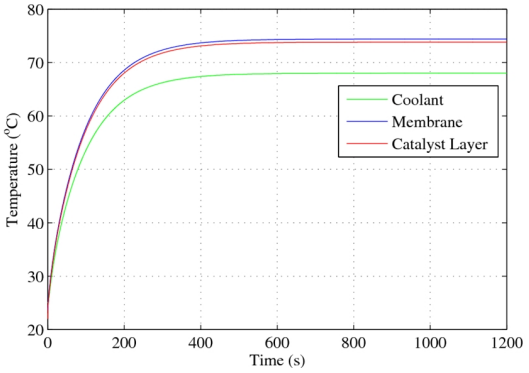

(a) Temperature dynamic graph.

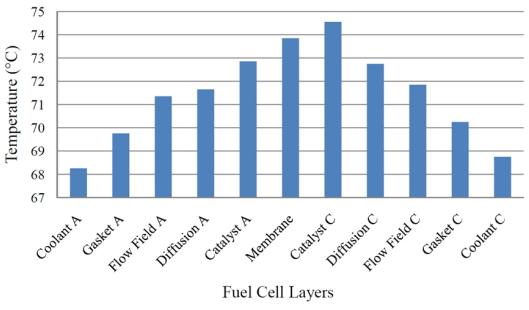

(b) Temperature results of the layers.

Fig. 16. Temperature in cell layers 20 min into the simulation.

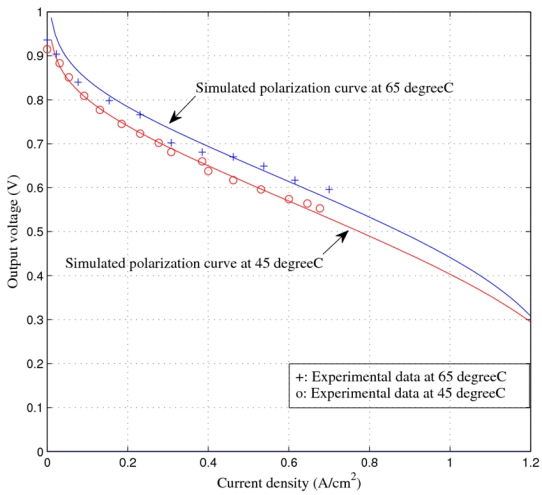

Fig. 17. Model validation of cell voltage using experimental data.

currently, this difference is limited to 4%.

In addition, the model validations of cell output voltage and power density were achieved using experimental data with a 1.2 kW Ballard Nexa fuel cell stack system. Experimental data extracted from the fuel cell stack system were converted to cell values considering the number and effective area of each cell, and power consumption in the stack system. In Fig. 15, the experimental data (cross) are laid on the three dimensional surface of the simulated voltage and power density curves.

C. Improved computation speed

Fig. 18 shows the real-time simulation computation time of the base fuel cell model. The computations of the base model were completed in an average of 16.9 μs. Fig. 19 shows the improvement in computation time using the proposed fast computation methods. Fig. 19 (a) shows the computation time when the model is modified using the MAC method. The results show a 38 % reduction in computation time using this method. Fig. 19 (b) and (c) show the computation time reduction for a model altered using the MS method for the multi-core simulator. The master block which computes the voltage loss model requires 4.4 μs, and the slave block which computes the thermal dynamic model of the fuel cell layers consumes 0.8 μs. The RL method saves an additional 25 % of the computation time of the thermal dynamic layer model, as shown in Fig. 19 (d).

Fig. 20 shows the performance of a complete simulation model including all the proposed methods of computation time reduction. The time consumptions of the voltage loss and thermal dynamic layer models are 2.8 μs and 0.6 μs, respectively. Consequently, the improvement in computation time brought about by the proposed model development approach is in the order of 80 %. Table II shows the computation times of the proposed methods.

VI. Conclusion

A computationally efficient electrical and thermal dynamic model of the PEM fuel cell for real-time simulation has been presented. The proposed model includes the electrochemical voltage generation and losses of the fuel cell and thermal dynamics of individual cell layers. The proposed model has been verified using experimental fuel cell data. By minimizing algebraic calculations (MAC), performing model separation (MS), and utilizing fuel cell structure symmetry (RL), the proposed fuel cell model's execution time is improved. The proposed model was tested and verified using the RT-LAB real-time simulator and an 80 % improvement in computation speed over the base model was achieved.

Extending the proposed model to include the dynamics of other fuel cell control subsystems is a natural continuation of this work. The work is also a first step in the development of fuel cell based power HIL architecture.

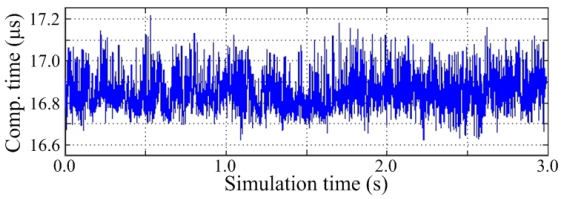

Fig. 18. Simulation computation time of the base model.

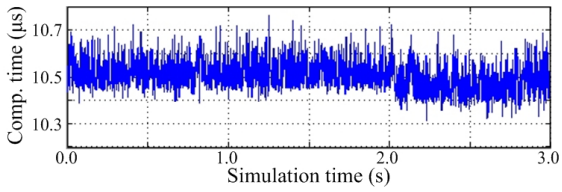

(a) MAC method.

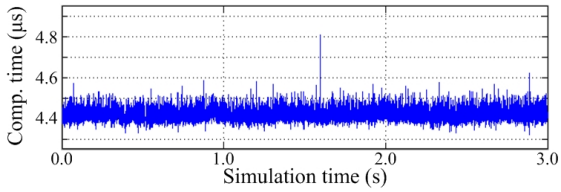

(b) MS master model.

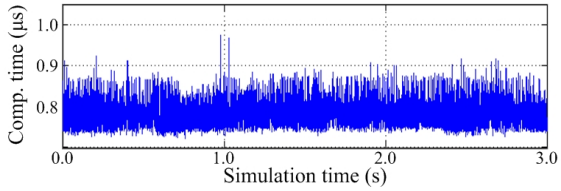

(c) MS slave model.

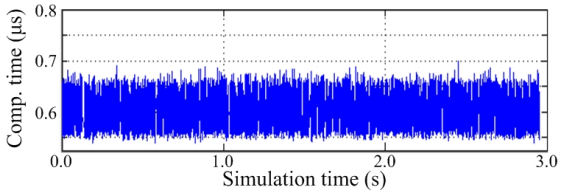

(d) RL slave model.

Fig. 19. Improved computation speed using the proposed methods.

Acknowledgment

This work was supported by a National Priorities Research Program (NPRP) grant from the Qatar National Research Fund

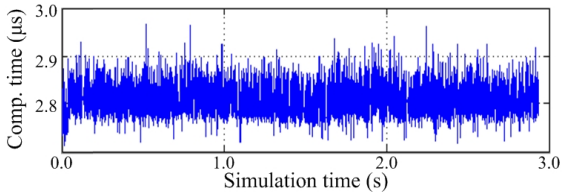

(a) Master voltage model.

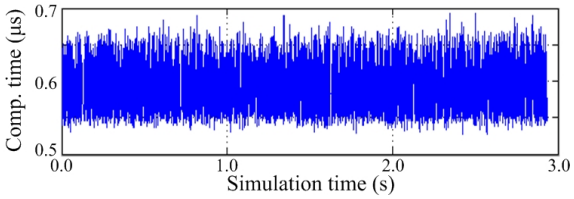

(b) Slave thermal dynamic model.

Fig. 20. Simulation computation time of the complete model.

TABLE II
COMPUTATION TIME OF THE PROPOSED METHODS (UNIT: μS)

Model	Base	MAC	MS	SL	Comp.
Serial	16.9	10.5	-	-	-
P. master	-	-	4.4	4.4	2.8
P. slave	-	-	0.8	0.6	0.6

(QNRF) and the National Research Foundation of Korea Grant funded by the Korean Government [NRF-2009-352-D00109].

REFERENCES

[1] B. D. Solomon and A. Banerjee, "A global survey of hydrogen energy research, development and policy," *Energy Policy*, Vol. 34, No. 7, pp. 781-792, May 2006.

[2] M. Tekin, D. Hissel, M.-C. Pera, and J. Kauffmann, "Energy management strategy for embedded fuel-cell systems using fuzzy logic," *IEEE Trans. Industrial Electronics*, Vol. 54, No. 1, pp. 595-603, Feb. 2007.

[3] C. A. Ramos-Paja, C. Bordons, A. Romero, R. Giral, and L. Martinez-Salamero, "Minimum fuel consumption strategy for pem fuel cells," *IEEE Trans. Industrial Electronics*, Vol. 56, No. 3, pp. 685-696, Mar. 2009.

[4] A. Emadi and S. S. Williamson, "Status review of power electronic converters for fuel cell applications," *Journal of Power Electronics*, Vol. 1, No. 2, pp. 133-144, Oct. 2001.

[5] I.-D. Park and S.-K. Kim, "A sliding mode observer design for fuel cell electric vehicles," *Journal of Power Electronics*, Vol. 6, No. 2, pp. 172-177, Apr. 2006.

[6] S. K. Kwon and K. F. A. Sayed, "Boost-half bridge single power stage PWM DC-DC converters for PEM-fuel cell stacks," *Journal of Power Electronics*, Vol. 8, No. 3, pp. 239-247, Jul. 2008.

[7] W. Lee, S.-J. Jang, S.-S. Kim, S.-W. Lee, and C. Y. Won, "A fuel cell generation system with a new active clamp sepic-flyback converter," *Journal of Power Electronics*, Vol. 9, No. 1, pp. 26-35, Jan. 2009.

[8] J. Hall and R. Kerr, "Innovation dynamics and environmental technologies: the emergence of fuel cell technology," *Journal of Cleaner Production*, Vol. 11, No. 4, pp. 459-471, Jun. 2003.

[9] X. Huang, Z. Zhang, and J. Jiang, "Fuel cell technology for distributed generation: An overview," *in Proceeding of IEEE International Symposium on Industrial Electronics*, pp. 1613–1618, 2006.

[10] A. Rowe and X. Li, "Mathematical modeling of proton exchange membrane fuel cells," *Journal of Power Sources*, Vol. 102, No. 1-2, pp. 82-96, Dec. 2001.

[11] J. M. Correa, F. A. Farret, L. N. Canha, and M. G. Simoes, "An electrochemical-based fuel-cell model suitable for electrical engineering automation approach," *IEEE Trans. Industrial Electronics*, Vol. 51, No. 5, pp. 1103–1112, Oct. 2004.

[12] S. Pasricha and S. R. Shaw, "A dynamic pem fuel cell model," *IEEE Trans. Energy Conversion*, Vol. 21, No. 2, pp. 484-490, Jun. 2006.

[13] Z. Zhang, X. Huang, J. Jiang, and B. Wu, "An improved dynamic model considering effects of temperature and equivalent internal resistance for pem fuel cell power modules," *Journal of Power Sources*, Vol. 161, No. 2, pp. 1062-1068, Oct. 2006.

[14] H. Wu, X. Li, and P. Berg, "Numerical analysis of dynamic processes in fully humidified pem fuel cells," *International Journal of Hydrogen Energy*, Vol. 32, No. 12, pp. 2022-2031, Aug. 2007.

[15] A. J. del Real, A. Arce, and C. Bordons, "Development and experimental validation of a pem fuel cell dynamic model," *Journal of Power Sources*, Vol. 173, No. 1, pp. 310-324, Nov. 2007.

[16] M. V. Moreira and G. E. da Silva, "A practical model for evaluating the performance of proton exchange membrane fuel cells," *Renewable Energy*, Vol. 34, No. 7, pp. 1734-1741, Jul. 2009.

[17] C. Siegel, "Review of computational heat and mass transfer modeling in polymer-electrolyte-membrane (pem) fuel cells," *Energy*, Vol. 33, No. 9, pp. 1331-1352, Sep. 2008.

[18] C. Lu-Ying, B. Diong, and R. S. Gemmen, "An improved small-signal model of the dynamic behavior of pem fuel cells," *IEEE Trans. Industry Applications*, Vol. 40, No. 4, pp. 970-977, Jul.-Aug. 2004.

[19] M. Uzunoglu and M. S. Alam, "Dynamic modeling, design, and simulation of a combined pem fuel cell and ultracapacitor system for standalone residential applications," *IEEE Trans. Energy Conversion*, Vol. 21, No. 3, pp. 767-775, Sep. 2006.

[20] T.-W. Lee, S.-J. Jang, H.-K. Jang, and C.-Y. Won, "A fuel cell generation system with a fuel cell simulator," *Journal of Power Electronics*, Vol. 5, No. 1, pp. 55-61, Jan. 2005.

[21] J.-G. Lim and S.-K. Chung, "Implementation of a fuel cell dynamic simulator," *Journal of Power Electronics*, Vol. 7, No. 4, pp. 336-342, Oct. 2007.

[22] X. Kong and A. M. Khambadkone, "Modeling of a pem fuel-cell stack for dynamic and steady-state operation using ann-based submodels," *IEEE Trans. Industrial Electronics*, Vol. 56, No. 12, pp. 4903-4914, Dec. 2009.

[23] W. K. Na and B. Gou, "Feedback-linearization-based nonlinear control for pem fuel cells," *IEEE Trans. Energy Conversion*, Vol. 23, No. 1, pp. 179-190, Mar. 2008.

[24] M. Meiler, O. Schmid, M. Schudy, and E. P. Hofer, "Dynamic fuel cell stack model for real-time simulation based on system identification," *Journal of Power Sources*, Vol. 176, No. 2, pp. 523-528, Feb. 2008.

[25] S.-Y. Choe, J.-W. Ahn, J.-G. Lee, and S.-H. Baek, "Dynamic simulator for a pem fuel cell system with a pwm dc/dc converter," *IEEE Trans. Energy Conversion*, Vol. 23, No. 2, pp. 669-680, Jun. 2008.

[26] C. Spiegel, *PEM fuel cell modeling and simulation using Matlab*, Academic Press/Elsevier, Chap. 2-10, 2008.

Jee-Hoon Jung was born in Suwon, Korea, in 1977. He received his B.S., M.S., and Ph.D. degrees from the Department of Electronic and Electrical Engineering, Pohang University of Science and Technology (POSTECH), Pohang, Korea, in 2000, 2002, and 2006, respectively. He was a Senior Research Engineer in the Digital Printing Division of Samsung Electronics Co., Ltd., Suwon, Korea from 2006 to 2009. He is currently a Postdoctoral Research Associate in the Electrical and Computer Engineering department of Texas A&M University at Qatar (TAMUQ). His research interests include dc-dc converters, switched mode power supplies, motor drives and diagnosis systems, digital control and signal processing algorithms, digitally controlled power electronics, and power conversions for renewable energy. Recently, he is researching on real-time and power hardware-in-the-loop (PHIL) simulations of the renewable energy sources. Dr. Jung is a member of the IEEE Industrial Electronics Society, IEEE Power Electronics Society, and the Korean Institute of Power Electronics (KIPE).

Shehab Ahmed was born in Kuwait City, Kuwait, in 1976. He received his B.Sc degree from the Department of Electrical Engineering, Alexandria University, CityAlexandria, Egypt in 1999; his MSc. and Ph.D degrees from the Department of Electrical and Computer Engineering at Texas A&M University in College Station, StateTX in 2000, and 2007 respectively. He was a senior development engineer at Schlumberger Technology Corporation, Sugarland, TX from 2001 to 2007. He is currently an Assistant Professor, in the Electrical and Computer Engineering Department of Texas A&M University at Qatar. His research interests are in the areas of mechatronics and energy conversion.